Magnetic Resonance Materials in Physics, Biology and Medicine
https://doi.org/10.1007/s10334-024-01154-x

RESEARCH ARTICLE

Quantifying H&E staining results, grading and predicting IDH mutation status of gliomas using hybrid multi-dimensional MRI

Wenbo Sun[1] · Dan Xu[2] · Huan Li[1] · Sirui Li[1] · Qingjia Bao[3] · Xiaopeng Song[4] · Daniel Topgaard[5] · Haibo Xu[1]

Received: 21 November 2023 / Revised: 26 February 2024 / Accepted: 29 February 2024

Abstract

Objective To assess the performance of hybrid multi-dimensional magnetic resonance imaging (HM-MRI) in quantifying hematoxylin and eosin (H&E) staining results, grading and predicting isocitrate dehydrogenase (IDH) mutation status of gliomas.

Materials and methods Included were 71 glioma patients (mean age, 50.17 ± 13.38 years; 35 men). HM-MRI images were collected at five different echo times (80–200 ms) with seven *b*-values (0–3000 s/mm^2). A modified three-compartment model with very-slow, slow and fast diffusion components was applied to calculate HM-MRI metrics, including fractions, diffusion coefficients and T2 values of each component. Pearson correlation analysis was performed between HM-MRI derived fractions and H&E staining derived percentages. HM-MRI metrics were compared between high-grade and low-grade gliomas, and between IDH-wild and IDH-mutant gliomas. Using receiver operational characteristic (ROC) analysis, the diagnostic performance of HM-MRI in grading and genotyping was compared with mono-exponential models.

Results HM-MRI metrics $F_{D\text{very-slow}}$ and $F_{D\text{slow}}$ demonstrated a significant correlation with the H&E staining results ($p < .05$). Besides, $F_{D\text{very-slow}}$ showed the highest area under ROC curve (AUC = 0.854) for grading, while *D*slow showed the highest AUC (0.845) for genotyping. Furthermore, a combination of HM-MRI metrics $F_{D\text{very-slow}}$ and $T2_{D\text{slow}}$ improved the diagnostic performance for grading (AUC = 0.876).

Discussion HM-MRI can aid in non-invasive diagnosis of gliomas.

Keywords Hybrid multi-dimensional MRI · Gliomas · Diffusion · IDH · Histologic

Abbreviations

CNS	Central nervous system
DWI	Diffusion weighted imaging
IDH	Isocitrate dehydrogenase
ADC	Apparent diffusion coefficient
LGG	Low-grade glioma
HGG	High-grade glioma
IDH-MUT	IDH-mutant glioma
IDH-WILD	IDH-wild glioma
HM-MRI	Hybrid multi-dimensional MRI
GRE	Gradient echo
TR	Repetition time
TE	Echo time
FOV	Field of view
FSE	Fast spin echo
FLAIR	Fluid-attenuated inversion recovery

Wenbo Sun and Dan Xu share the first authorship.

✉ Daniel Topgaard
daniel.topgaard@fkem1.lu.se

✉ Haibo Xu
xuhaibo@whu.edu.cn

[1] Department of Radiology, Zhongnan Hospital of Wuhan University, Wuhan 430071, Hubei, People's Republic of China

[2] Department of Nuclear Medicine, Zhongnan Hospital of Wuhan University, Wuhan 430071, Hubei, People's Republic of China

[3] State Key Laboratory of Magnetic Resonance and Atomic and Molecular Physics, National Center for Magnetic Resonance in Wuhan, Wuhan Institute of Physics and Mathematics, Innovation Academy for Precision Measurement Science and Technology, Chinese Academy of Sciences, Wuhan 430071, Hubei, People's Republic of China

[4] Central Research Institute, United-Imaging Healthcare, Shanghai, China

[5] Department of Chemistry, Lund University, P.O.B. 124, 221 00 Lund, Sweden

Published online: 05 April 2024

EES	Extravascular extracellular space
BBB	Brain-blood barrier
ROI	Regions of interest
IHC	Immune-histochemical
ROC	Receiver operating characteristic
AUC	Area under the receiver operating characteristic curve
LR	Logistic regression
WHO	World Health Organization
H&E	Hematoxylin and eosin
AQP4	aquaporin-4

Introduction

Glioma is the most common and malignant tumor in the central nervous system (CNS) [1]. The diagnosis of gliomas is based on an integrated morphological and molecular analysis [2]. The morphological analysis mainly relies on hematoxylin and eosin (H&E) staining, which is the base for histological grading. The molecular analysis is dependent on key molecular biomarkers, among which the isocitrate dehydrogenase (IDH-1 and IDH-2) gene mutations play the most important role [3]. According to the 2021 World Health Organization (WHO) classification, despite the absence of high-grade histopathologic features, an IDH-wild glioma might be also diagnosed as grade 4 due to its highly aggressive pattern of growth [4]. However, above integrated pathological diagnosis needs invasive procedures, including surgery or needle biopsy [5]. Therefore, developing non-invasive diagnosis tools is essential.

Magnetic resonance imaging (MRI) is a useful imaging tool for the non-invasive diagnosis of gliomas [6]. Diffusion and relaxation are two basic concepts of MRI [7]. Diffusion weighted imaging (DWI), which characterizes the random walk of water molecules within the tumor microenvironment [8], has been shown to be effective in grading and genotyping of gliomas [9–11]. For instance, the most commonly used DWI metric apparent diffusion coefficient (ADC) can be used to grade gliomas [9, 10] and detect IDH mutation status [10, 11]. Relaxation MRI, which provides quantitative transverse (T2) and longitudinal (T1 and T1ρ) relaxation maps, has also been applied for the diagnosis of gliomas [12–17]. Among these maps, T2 map has been used for grading gliomas [12] and genotyping [13], and is thought to be beneficial for identifying regions of infiltration in the clinic. However, despite the usefulness of above diffusion and relaxation MRI metrics, they only provided the voxel-averaged information. Thus, it is difficult to directly correlate these diffusion and relaxation metrics with the microstructure or compositions of tumor tissues at a sub-voxel scale. Furthermore, because DWI images are both diffusion and T2 weighted, variations in T2 relaxation time always cause some difficulty in explaining the changes of the diffusion signal [18]. Typically, the "T2-shine-through" (due to T2 prolongation) and "T2-blackout" (due to T2 shortening and susceptibility) effects remain pitfalls when using DWI for clinical diagnosis [19]. As a result, it is critical to quantify and resolve diffusion and relaxation properties at the sub-voxel level, which might provide substantial benefits in the clinic.

Recently, hybrid multi-dimensional MRI (HM-MRI), a novel sub-voxel imaging tool, has showed potential in diagnosing prostate cancer [20]. HM-MRI simultaneously measures changes in ADC and T2 values as a function of echo time (TE) and diffusion weighting (b-value), respectively, and uses these changes to depict tissue compositions inside a voxel by assuming three different components (lumen, stroma and epithelium) [20]. It was found that fractions of multiple components measured by HM-MRI were strongly related to histological percentages of different prostate cancer tissues [21]. Besides, HM-MRI measured fractions and quantitative histological evaluations had equivalent performance for differentiating and locating malignant lesions [21]. Moreover, HM-MRI has been suggested to have advantages over multi-parametric MRI (T2 + ADC) in diagnosing prostate cancer [22]. However, to date, HM-MRI has not been applied in evaluating gliomas. Different from prostate cancer studies, challenge emerges when identifying boundaries between tumor cells and stroma cells in glioma tissues. Thus, the clinical value of HM-MRI in diagnosing gliomas requires further validation.

Due to the ability to image at sub-voxel scale, we hypothesized that HM-MRI might aid in the non-invasive detection of histological features of gliomas tissues. We also expected that HM-MRI might help in locating tumor lesions by separating the T2 effect in DWI. Besides, HM-MRI might improve the diagnostic performance of gliomas beyond the use of mono-exponential T2 or diffusion models or their combination. Thus, the objective of this study is to find the correlation between HM-MRI metrics with quantitative H&E staining results in glioma tissues, and to evaluate the diagnostic performance of HM-MRI metrics in grading and predicting IDH mutation status of gliomas, by comparing it with mono-exponential T2 and diffusion models.

Materials and methods

This prospective study was approved by the Institutional Review Board of our hospital (Ethics number 2020109), and informed consent was obtained from all enrolled subjects. From October 2020 to February 2023, a total of 153 individuals were recruited from the neurosurgery department. The inclusion criteria were as follows: (1) age between 18 and 80 years old; (2) suspected to have intracranial tumors; (3)

absence of MRI contraindications; (4) no relevant treatment history, including surgery, chemotherapy, or radiotherapy; (5) scheduled to receive surgical treatment within a week after the HM-MRI. The exclusion criteria were as follows: (1) inadequate image quality due to significant motion or magnetic susceptibility artifacts ($n = 1$); (2) pathological confirmation of non-glioma tumor type ($n = 81$). Please refer to Fig. 1 for the patient selection process flowchart.

MRI protocol

All MRI examinations were conducted using a clinical 3.0 T scanner (uMR 790, United Imaging Healthcare) equipped with a 24-channel phased-array head-neck coil. HM-MRI was acquired through a single-shot echo-planar imaging sequence with a 180° refocusing pulse and the following parameters: field of view (FOV) = 200 × 230 mm^2, repetition time (TR) = 2000 ms, TE = 80, 100, 120, 150, 200 ms, slice thickness = 5 mm, slice number = 7, acceleration = 3.0, gap = 0, flip angle (FA) = 90°, resolution in plane = 1.44 × 1.44 mm^2, matrix = 139 × 160, interpolation for reconstruction = 2, and 7 *b*-values (0_1, 100_1, 200_1, 400_1, 800_2, 1500_3, 3000_6 s/mm^2, while the subscript of *b*-values indicated the number of average times at the corresponding *b*-value), total acquisition time = 8min20sec (for each TE, acquisition time = 1min40sec). Other routine MRI protocols included a 3D T1-weighted gradient echo (T1w-GRE) sequence (TR/TE = 7.2/3.1 ms, FA = 10°, resolution = 1 mm isotropic, matrix = 240 × 256 × 256), a 3D T2-weighted fluid-attenuated inversion recovery (T2w-FLAIR) sequence (TR/TE = 6000/430 ms, TI = 2420 ms, resolution = 1 mm isotropic, matrix = 240 × 256 × 256), and a 2D T2-weighted fast spin echo sequence (T2w-FSE) (FOV = 200 × 230 mm^2, TR/TE = 5385/95 ms, slice thickness = 5 mm, slice number = 23, gap = 20%, resolution in plane = 0.45 × 0.45 mm^2, matrix = 445 × 512), followed by a contrast-enhanced T1w-GRE scan.

Data fitting algorithms

All HM-MRI data were analyzed using an in-house program developed in MATLAB (2023a, MathWorks). T2 maps were calculated from multi-echo T2-weighted images using a mono-exponential signal decay model, which was based on images acquired at *b*-values of 0 s/mm^2 at all TEs (80, 100, 120, 150, and 200 ms).

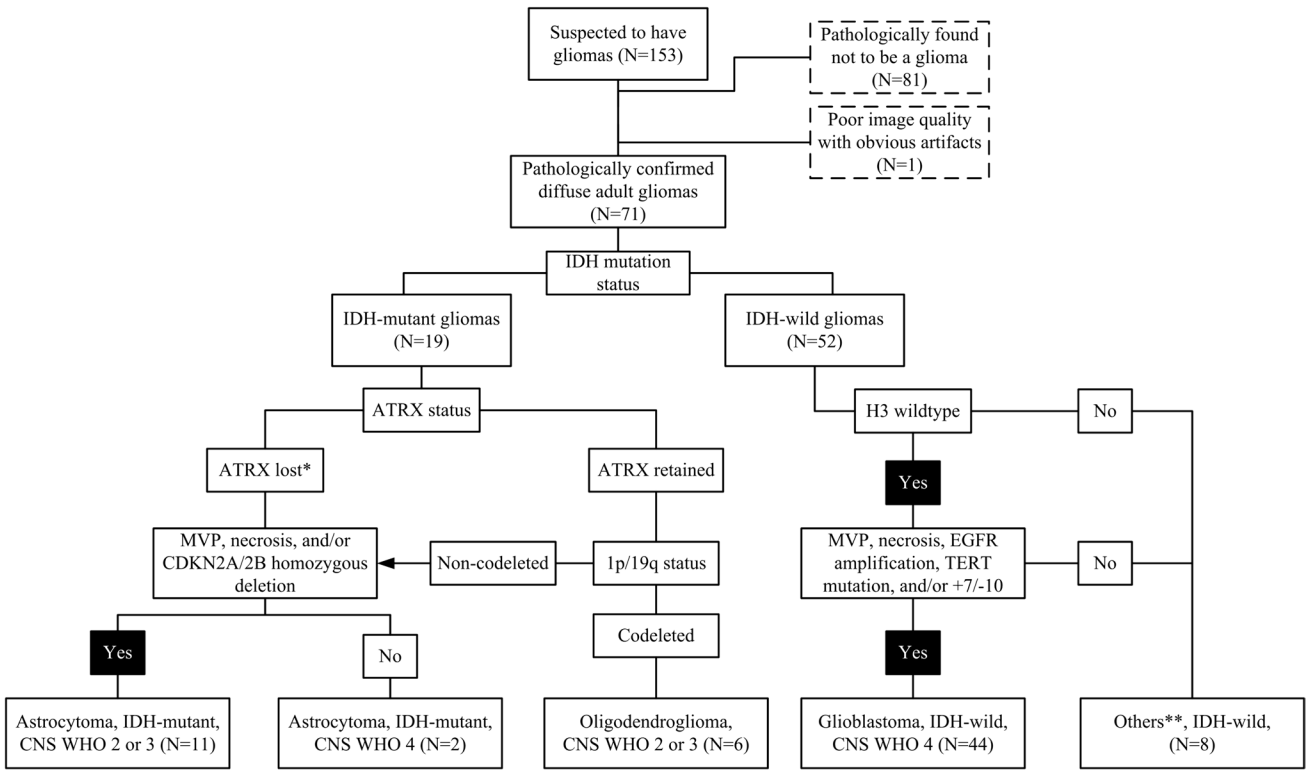

Fig. 1 The flowchart from initial retrieval to final study cohort and the algorithm of the glioma classification utilized in our study. The algorithm is based on the WHO CNS5 2021 classification of gliomas. *ATRX lost is enough for the diagnosis of IDH-mutant astrocytoma, and the detection of 1p/19q is not necessary. **IDH-wild gliomas without molecular features of a glioblastoma and sufficient data for other classification

$$S = S_0 * \exp(-\mathrm{TE}/\mathrm{T2})$$

where S is the signal at each TE and S_0 is the extrapolated signal TE = 0 ms.

The ADC maps were calculated from diffusion data acquired at TE = 80 ms using mono-exponential signal decay:

$$S = S_0 * \exp(-b * \mathrm{ADC})$$

where S_0 is the signal intensity without diffusion (b-value = 0 s/mm^2), S is the signal intensity at a certain b-value.

We modeled the signal attention of the HM-MRI data from three components: *D*very-slow, *D*slow and *D*fast. The "*D*very-slow" component is considered to represent water molecules strictly limited in cells with a "zero-ADC" [23, 24]. Then, the modified three-component model is expressed as follows:

$$-b * D\mathrm{sl}$$

$$\text{ery-slow} + F_{D\mathrm{slow}} + F_{D\mathrm{fast}} =$$

where $F_{D\text{very-slow}}$, $F_{D\text{slow}}$, and $F_{D\text{fast}}$ are the volume fractions of each component within a voxel, $\mathrm{T2}_{D\text{very-slow}}$, $\mathrm{T2}_{D\text{slow}}$, and $\mathrm{T2}_{D\text{fast}}$ are the T2 values for each component, while *D*slow and *D*fast are the diffusion coefficients for the slow and fast components. S is the signal intensity at each combination of TEs and b-values; and ɔ is the extrapolated signal intensity at TE = 0 ms calculated with the above mono-exponential T2 model. All metrics were obtained from voxel-by voxel fitting using the Nonlinear Least Squares (*lsqnonlin*) method of the *Optimization Toolbox*. Before the HM-MRI fitting, some initial values and constraints should be set. In this study, the lower and upper limits for $F_{D\text{very-slow}}$ is [0, 0.33], for $F_{D\text{slow}}$ is [0, 1], and for $F_{D\text{fast}}$ is [0, 1], while the initial values for $F_{D\text{very-slow}}$, $F_{D\text{slow}}$, and $F_{D\text{fast}}$ are 0.1, 0.7, 0.2, respectively. It should also be noted that the fitting included the constraint r_1. The lower and upper limit for *D*slow is [0.00001 mm^2/s, 3.0 mm^2/s], for *D*fast is [1.0 mm^2/s, 20 mm^2/s], and the initial values for *D*slow and *D*fast is 1.0 mm^2/s and 5.0 mm^2/s, respectively. The overlap [1.0 mm^2/s, 3.0 mm^2/s] of the range for *D*slow and *D*fast is necessary in our study, since we considered an exchange of the water molecules between the extravascular extracellular space (EES) and vessels may exist due to damaged brain-blood barrier (BBB) in gliomas. As for $\mathrm{T2}_{D\text{very-slow}}$, $\mathrm{T2}_{D\text{slow}}$, and $\mathrm{T2}_{D\text{fast}}$, the lower and upper limit is [0 ms, 2500 ms], and the initial values are 50 ms, 100 ms and 500 ms, respectively. To explore the possible T2 of different component, especially for the "zero-ADC" component, here we use the same lower and upper T2 limit for all components. The fitting code of this study can be downloaded at https://github.com/sysunwenbo/HM-MRI.

With the open-resource tool ITK-SNAP [25], regions of interest (ROIs) were delineated on b = 800 s/mm^2 images by referencing routine MRI images (T2w-FSE, T2w-FLAIR, and enhanced T1-weighted images) to cover solid parts of gliomas and exclude obvious vessels, hemorrhage, necrosis, cystic, and edema areas. Two radiologists (with five and ten years of clinical experience) were asked to draw ROIs blinded to pathological diagnosis and reach a consensus. Only one ROI was used for analysis for each subject.

Pathological examination

For H&E staining, glioma samples were fixed in 4% paraformaldehyde, embedded into paraffin and sliced into 4-μm-thick histological sections. For the IDH (including IDH-1 and IDH-2) gene mutation status, Sanger sequencing was performed. Other important molecular biomarkers were identified by immune-histochemical (IHC) analysis or Sanger sequencing. The classification of gliomas was performed by an experienced neuropathologist with 10 years of clinical experience following the latest WHO 2021 guidance for CNS tumors. The grading and classification results are presented in Table 1.

Table 1 The clinic pathological characteristics and molecular features of patient cohort

Tumor type and grade	Age (years)	Gender	
		Male	Female
Astrocytoma, grade 2 or 3, IDH-mutant	42.73 ± 11.96	5	6
Astrocytoma, grade 4, IDH-mutant	47.5 ± 12.02	1	1
Oligodendroglioma, grade 2 or 3, IDH-mutant	40.00 ± 10.45	2	4
Glioblastoma, grade 4, IDH-wild	55.36 ± 12.61	22	20
Other[a], grade 2 or 3[b], IDH-wild	43.2 ± 10.73	5	5

IDH, isocitrate dehydrogenase;

[a]IDH-wild gliomas without molecular features of a glioblastoma and enough molecular information for other classification, especially for pediatric-type diffuse gliomas in young adults

[b]In the dataset, the other cohort were graded as 2 or 3 based on the histologic features

It is important to highlight that the quantitative analysis and interpreting for H&E staining in our study significantly differ from previous study in prostate cancer [20]. To quantify the H&E staining results, an automated extraction method was applied: this involved utilizing a multi-channel RGB threshold tool in ImageJ to separate tissues, enabling visual extraction of three distinct areas, including cell nuclear area, a combination of cytoplasm and extracellular matrix areas, as well as background area (containing fluid in EES and vessel areas). This definition arises due to the difference between glioma tissues and prostate cancer tissues. It is challenging to distinguish between the stroma and tumor cells within glioma tissues using H&E staining, as well as to separate the extracellular matrix area from the cytoplasm area. Hence, the cytoplasm and extracellular matrix areas were considered as one compartment. To quantify the H&E staining results, the following steps were followed:

Step1: choose a representative H&E staining image and an ROI.

Step2: using the "***Split Channel***" function in the ImageJ.

Step3: using the "***Threshold***" function for red channel in the ImageJ to calculate the percentage of cell nuclear area (f1).

Step4: using the "***Threshold***" function for green channel in the ImageJ to calculate the percentage of a combination of cell nuclear area (f1) and cytoplasm and extracellular matrix areas (f2).

Step5: the percentage of background area f3 equals to 1-f1-f2.

Step6: repeat the preceding steps three times for three ROIs to obtain the average value of f1, f2, and f3.

Statistical analysis

All parameters were presented in the text as mean ± standard deviation (SD). The Mann–Whitney U test was used to compare all metrics between high-grade and low-grade gliomas, and between IDH-wild and IDH-mutant gliomas. The normal distribution of all parameters was confirmed using the Kolmogorov–Smirnov test. Receiver operating characteristic (ROC) analysis was performed for all imaging metrics and their combinations, and the area under the ROC curve (AUC) for grading gliomas and predicting IDH mutation status was computed. The optimal cutoff points were determined using the highest Youden index to achieve the best sensitivity–specificity balance. A forward binary logistic regression (LR) analysis was utilized to identify the best set of predictors with default entry and removal criteria of 0.05 and 0.10. The Pearson correlation analysis was performed between the fractions derived from HM-MRI as well as ADC and the percentages derived from quantitative H&E staining results. Statistical analysis was conducted using SPSS v24.0 (Chicago, IL) and the R package v4.2.0 (R Core Team, 2022). A p-value of $< .05$ indicated statistical significance.

Results

Table 1 indicates that the study included a total of 71 subjects (35 males and 36 females; age range 19–78 years, mean age 50.17 ± 13.38 years), consisting of 18 low-grade gliomas and 53 high-grade gliomas (19 IDH-mutant cases and 52 IDH-wild cases). Figure 2a, b illustrates the routine clinical and diffusion images of a low-grade IDH-mutant case and a high-grade IDH-wild case, respectively. It was obvious that compared to the high-grade IDH-wild case, the low-grade IDH-mutant example exhibited a lower $F_{D\text{very-slow}}$ and a higher $F_{D\text{slow}}$. Figure 2 also indicates that HM-MRI was more effective in locating tumor lesions than the mono-exponential DWI. For the IDH-mutant case in Fig. 2a**,** if we didn't look at the T2 image, it is quite easy to identify the high signal intensity part (white arrow) at the b800 images as a restricted diffusion region. Nevertheless, by looking at HM-MRI metrics $T2_{D\text{very-slow}}$ and $T2_{D\text{slow}}$, it is quite easy to confirm it is a typical "T2-shine-through" case**.** For the IDH-wild high grade case in Fig. 2b, when we looking at the b800 images, it was obvious that there is a low signal intensity part (white arrow) at the b800 images which might be regarded as edema region with slightly increased ADC. However, when we reference the HM-MRI metrics $F_{D\text{very-slow}}$ and $F_{D\text{slow}}$, we found no significant difference between this low intensity part and other parts of the tumors. Through verification using the HM-MRI metrics $T2_{D\text{very-slow}}$ and $T2_{D\text{slow}}$, this area was identified as a "T2-blackout" region.

Correlation of metrics with quantitative H&E results

Figure 3 shows an example of segmented H&E staining images used for quantitative histologic evaluations of the two glioma cases mentioned above. As shown in Table 2, we found significant correlations between HM-MRI metric $F_{D\text{very-slow}}$ with the percentage of cell nuclear area (rho = 0.270, $p < .05$) and the combination of cytoplasm and extracellular matrix areas (rho = −0.289, $p < .05$). Besides, the HM-MRI metric $F_{D\text{slow}}$ showed significant correlation with the percentage of cell nuclear area (rho = −0.305, $p < .01$) and the combination of cytoplasm and extracellular matrix areas (rho = 0.344, $p < .01$).

The Bland–Altman and linear regression plots both suggested a good correlation between $F_{D\text{very-slow}}$ and the percentage of the cell nuclear area and $F_{D\text{slow}}$ with the combination of cytoplasm and extracellular matrix areas, as shown in Fig. 4. However, as shown in Table 2, no significant correlation between the quantified H&E findings with the ADC,

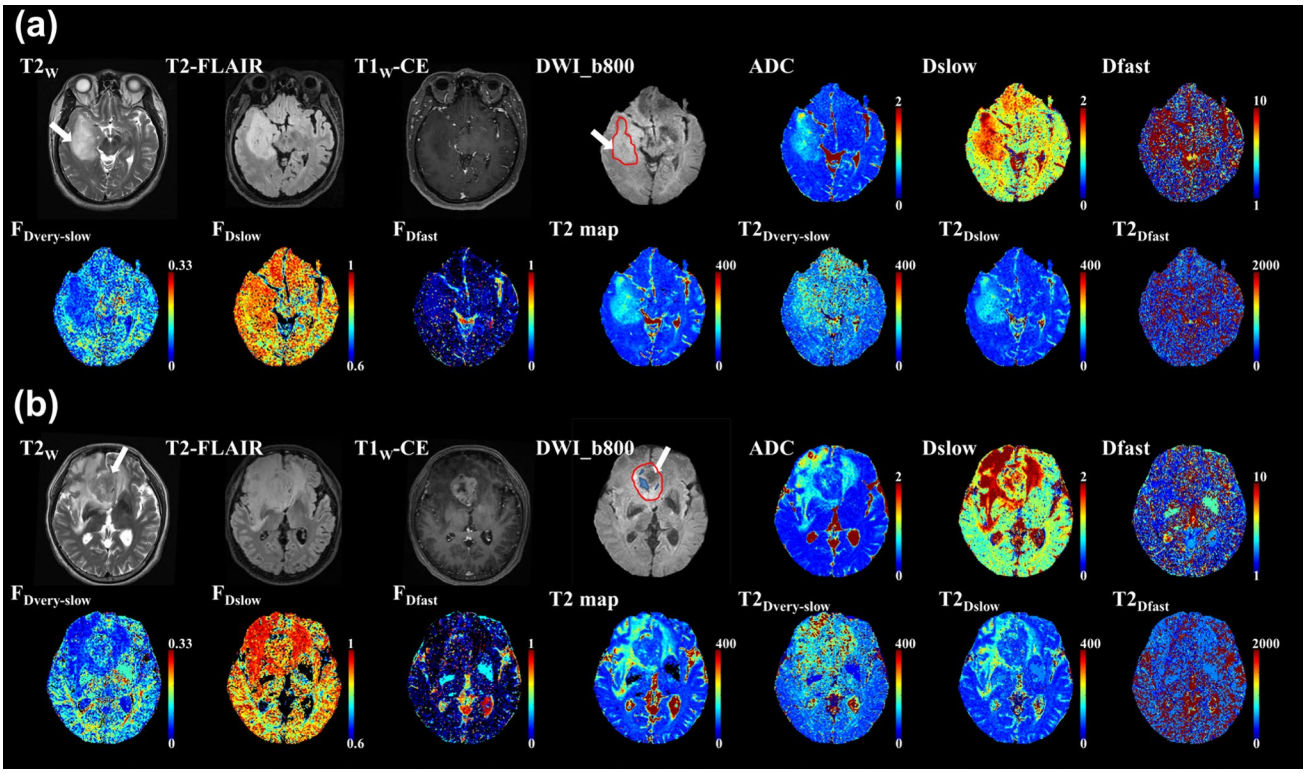

Fig. 2 **a** Images obtained from a 45-year-old male with an isocitrate dehydrogenase 1 (IDH-1) mutant astrocytoma of WHO grade 2. Regions of interest (red circle) are marked on parametric maps and co-registered to the $b = 800$ s/mm^2 map. The T2-shine-through region was shown in T2w-FSE and b800 images (the white arrow), with a higher signal intensity than the normal brain tissues. **b** Images obtained from a 56-year-old male with glioblastoma, WHO grade 4. Regions of interest (red circle) are marked on parametric maps and co-registered to the $b = 800$ s/mm^2 map. Obvious vessels, necrosis, and edema areas were marked as blue regions and removed during the statistical analysis. The T2-blackout region is shown in T2w-FSE and b800 images (the white arrow), with a lower signal intensity than the other part of the tumors. The unit for parameters ADC, *D*slow, and *D*fast are $\times 10^{-3}$ mm^2/s, while the unit for global T2, $T2_{Dvery\text{-}slow}$, $T2_{Dslow}$, $T2_{Dfast}$ are milliseconds (ms). The $F_{Dvery\text{-}slow}$, F_{Dslow} and F_{Dfast} are unitless

and the percentage of background areas with the F_{Dfast} was found.

Comparison of metrics for grading gliomas

As shown in Table 3, a significant difference in the combination of cytoplasm and extracellular matrix areas was found between high-grade and low-grade gliomas ($p < .05$). In Table 4**,** except for the HM-MRI metrics F_{Dfast}, *D*fast and $T2_{Dfast}$, all metrics significantly differentiate high-grade gliomas and low-grade gliomas. High-grade gliomas had significantly higher $F_{Dvery\text{-}slow}$ compared to low-grade gliomas, while F_{Dslow}, *D*slow, $T2_{Dvery\text{-}slow}$, $T2_{Dslow}$, and global T2 and ADC derived from mono-exponential models, were all significantly lower in high-grade gliomas ($p < .05$). Moreover, Table 5 highlights that $F_{Dvery\text{-}slow}$ achieved the highest AUC (0.854) for grading gliomas. Using the LR analysis, we discovered that the combination of HM-MRI metrics $F_{Dvery\text{-}slow}$ and $T2_{Dslow}$ enhanced the AUC to 0.876. Figure 5a, b displays the ROC curves for grading gliomas using different metrics.

Comparison of metrics for predicting IDH mutation status

As shown in Table 3, no significant difference in quantitative H&E staining results was found between IDH-mutant and IDH-wild groups. However, in Table 4, it is evident that all metrics, except for the HM-MRI metrics F_{Dfast} and *D*fast, were able to significantly differentiate IDH-mutant gliomas from IDH-wild gliomas. Specifically, the IDH-wild gliomas had significantly higher $F_{Dvery\text{-}slow}$ value compared to the IDH-mutant gliomas, while F_{Dslow}, *D*slow, $T2_{Dvery\text{-}slow}$, $T2_{Dslow}$, $T2_{Dfast}$, global T2 and ADC were all significantly lower in IDH-wild gliomas ($p < .05$). By performing the LR analysis, the *D*slow alone still showed the highest AUC (0.845) for predicting IDH mutation status. Figure 5c, d displays the ROC curves for predicting IDH mutation status using different metrics.

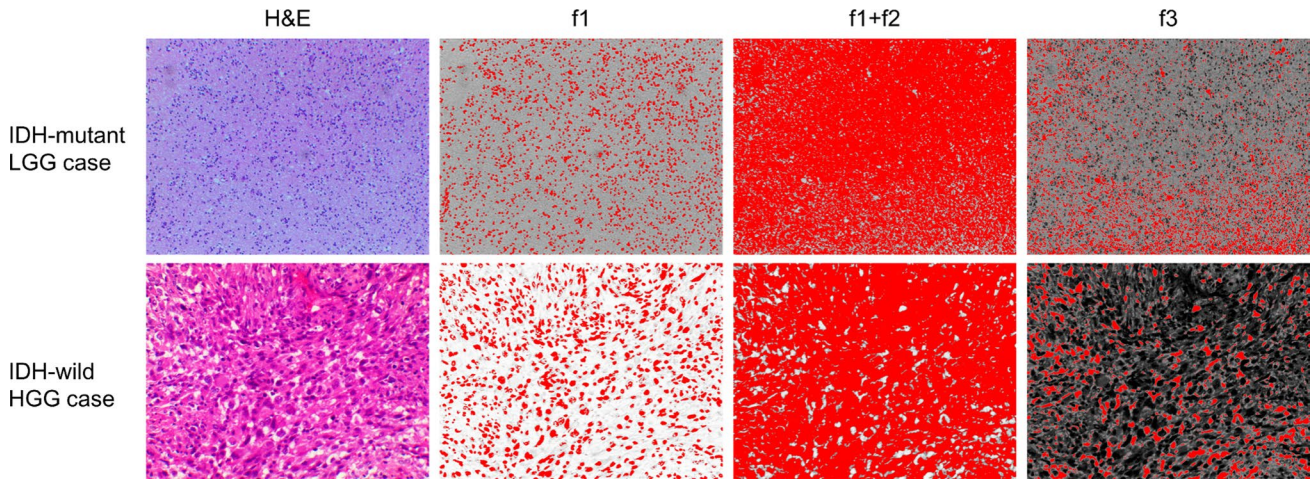

Fig. 3 Representative H&E staining images (resolution 400x) for quantitative histologic evaluation in which tissue was segmented into cell nuclei area (f1), a combination of cell nuclei area, cytoplasm and extracellular matrix areas (f1 + f2), and background area (f3) for two patients shown in Fig. 2, respectively. The tissue composition estimated using hybrid multidimensional MRI and quantitative histologic evaluation showed good agreement for both IDH mutant case (HM-MRI vs histology: cell nuclei area, 6.41% vs 11.54%; cytoplasm and extracellular matrix areas, 84.23% vs 72.10%; and background area, 9.35% vs 16.36%) and IDH wild case (cell nuclei area, 9.80% vs 17.29%; cytoplasm and extracellular matrix areas, 77.63% vs 66.67%; and background area, 12.58% vs 16.04%). H&E = hematoxylin and eosin

Table 2 Pearson rho values between the ADC and HM-MRI derived fractions with percentages of different H&E staining areas among all subjects

Metrics	Cell nuclear area, f1 (%)	Cytoplasm and extracellular matrix areas, f2 (%)	Background area, f3 (%)
ADC	−0.151	0.144	−0.035
$F_{D\text{very-slow}}$	0.270*	−0.289*	0.111
$F_{D\text{slow}}$	−0.305**	0.344**	−0.152
$F_{D\text{fast}}$	0.177	−0.210	0.104

*Correlation was found be significant ($p < .05$)

**Correlation was found be significant ($p < .01$)

Discussion

The objective of this study was to evaluate the efficacy of HM-MRI in quantifying H&E staining results, grading and predicting IDH mutation status. Our results revealed $F_{D\text{very-slow}}$ and $F_{D\text{slow}}$ had modest correlation with the quantitative H&E staining results. Besides, we found that HM-MRI metric $F_{D\text{very-slow}}$ exhibited the highest AUC for grading gliomas, and HM-MRI metric *D*slow exhibited the highest AUC for genotyping, outperforming the mono-exponential T2 or diffusion models, or their combination. Furthermore, integrating the HM-MRI metrics $F_{D\text{very-slow}}$ and $T2_{D\text{slow}}$ resulted in improvement of the AUC for grading gliomas. Altogether, these findings suggest that HM-MRI could potentially be used as a valuable tool for diagnosing gliomas in clinical settings.

In this study, a modified three-compartment model with the "zero-ADC" assumption was utilized to fit the HM-MRI data, which distinguished itself from the general three-compartment model used in prior HM-MRI studies [20][21]. Our decision to use this modified model and the "zero-ADC" assumption was inspired by two diffusion studies conducted on normal brain tissue and gliomas [23, 24]. Zeng et al. [23] demonstrated that the modified three-compartment model provides better fits for diffusion data compared to the original three-compartments model in white matter. Cao et al. [24] suggested that the "zero-ADC" component may be linked to the expression of aquaporin-4 (AQP4) and changes in membrane permeability in tumor cells of gliomas. However, both Zeng et al. and Cao et al. did not perform correlation analysis with histologic findings.

In our study, we investigated the correlations between HM-MRI metrics and quantitative H&E evaluations. We did observe a positive correlation between the HM-MRI metric $F_{D\text{very-slow}}$ with the percentage of cell nuclear area in H&E staining images. Our findings suggested that the "zero-ADC"

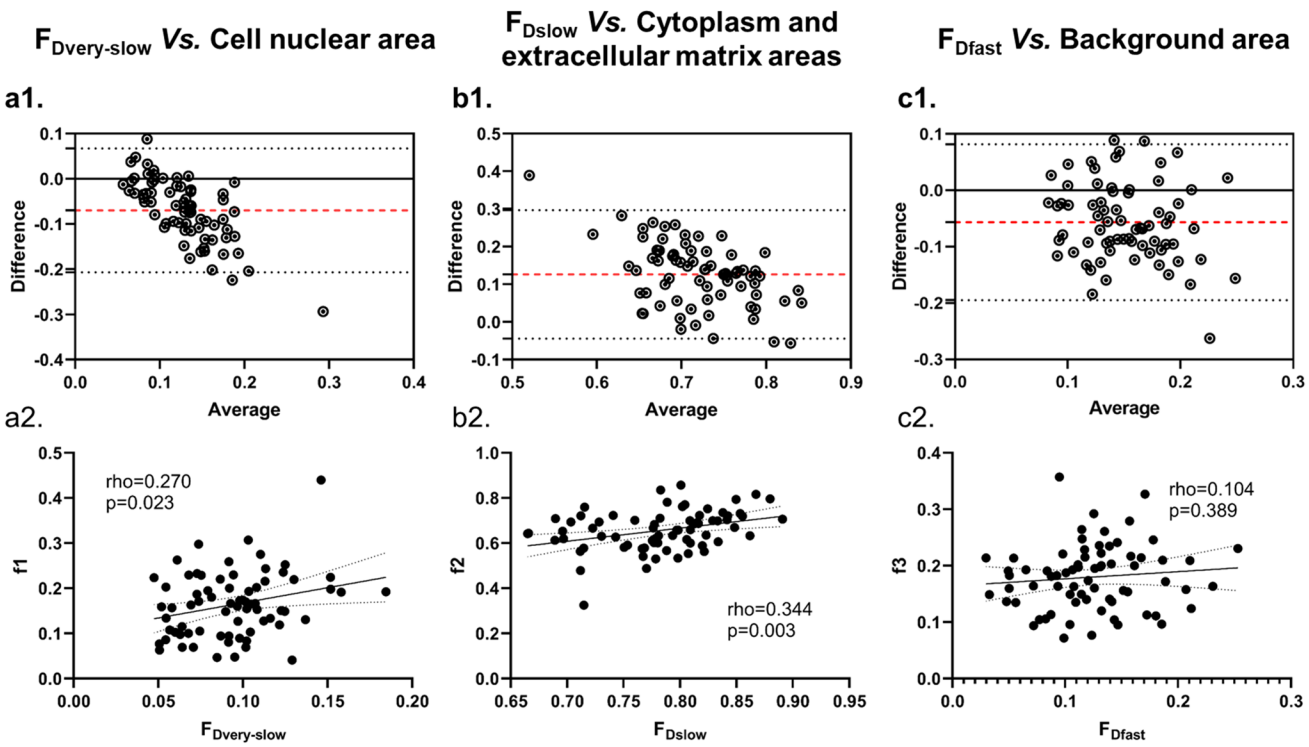

Fig. 4 Bland–Altman plots of differences in histologic measurements (*y*-axis) against the HM-MRI measurements (x-axis), with a mean absolute difference (bias) (red dashed lines) and 95% confidence intervals of the mean difference (limits of agreement, LOA) (black dashed lines) (**a1**, **b1**, **c1**), and the corresponding linear regression plots (**a2**, **b2**, **c2**)

Table 3 Mean values ± SD of percentages of different H&E staining areas between the HGGs and LGGs group, and between the IDH mutant and the IDH wild group

H&E results	HGGs	LGGs	*p*-value	IDH-WT	IDH-MUT	*p*-value
Cell nuclear area, f1 (%)	17.17 ± 7.36	14.07 ± 6.39	.128	16.76 ± 7.20	15.33 ± 7.30	.467
Cytoplasm and extracellular matrix areas, f2 (%)	64.09 ± 8.64	70.19 ± 8.46	.011*	64.94 ± 9.08	67.53 ± 8.49	.296
Background area, f3 (%)	18.74 ± 5.23	15.73 ± 6.79	.050	18.29 ± 5.68	17.13 ± 6.05	.459

HGGs high grade gliomas, *LGGs* low grade gliomas, *IDH* isocitrate dehydrogenase,*IDH-WILD* IDH wild type gliomas, *IDH-MUT* IDH mutant type gliomas,

*Significant difference was found ($p < .05$)

component might represent the highly restricted water molecules within tumor cells, predominantly located in the cell nuclei, rather than the changes in membrane permeability suggested by Cao et al. [24]. A previous pathological study showed that the fraction of cell nuclear area exhibited positive correlation with glioma grades [26], which could support our finding in $F_{Dvery\text{-}slow}$. Additionally, we discovered a higher value of $T2_{Dvery\text{-}slow}$ than $T2_{Dslow}$, which may confirm our idea about the "zero-ADC" component, as water molecules positioned in cell nucleus may not also have a very short T2. Regarding the "*D*slow" component, it was found that high-grade gliomas had a significantly smaller combination of cytoplasm and extracellular matrix regions than low-grade gliomas, and that F_{Dslow} and the cytoplasm and extracellular matrix areas correlated the most (rho = 0.344). Although F_{Dslow} was suggested to be related with the fraction of the EES in pervious diffusion studies [24, 27], the range of *D*slow and $T2_{Dslow}$ together in this HM-MRI study indicated the F_{Dslow} might be more correlated with the percentage of stroma areas, which was consistent with the previous prostate cancer studies [20–22]. Given the higher level of $F_{Dvery\text{-}slow}$, the much smaller stroma areas in high-grade gliomas compared to low-grade gliomas could be attributed to increased intracellular space of tumor cells, high interstitial fluid pressure, and angiogenesis. The F_{Dfast} showed no significant difference across groups, which could be attributed to the fact that we selected a lower limit of 1.0 mm^2/s for this component during the HM-MRI fitting. Thus, the "*D*fast"

Table 4 Mean values ± SD of each MRI-derived parameters of different models between HGGs group and LGGs group, and between IDH-mutant group and IDH-wild group

Model	Metrics	HGGs	LGGs	*p*-value	IDH-WT	IDH-MUT	*p*-value
Mono-exp	ADC	0.42 ± 0.11	0.59 ± 0.18	.000***	0.41 ± 0.10	0.60 ± 0.18	.000***
	$T2_{global}$	110.29 ± 25.09	136.72 ± 24.08	.000***	109.88 ± 23.92	136.45 ± 26.84	.000***
HM-MRI	$F_{Dvery\text{-}slow}$	10.27 ± 2.65	6.87 ± 2.04	.000***	10.26 ± 2.64	7.06 ± 2.27	.000***
	F_{Dslow}	77.30 ± 5.06	81.07 ± 5.18	.010*	77.28 ± 5.36	80.92 ± 4.27	.014*
	F_{Dfast}	12.43 ± 4.89	12.07 ± 4.25	.781	12.46 ± 4.98	12.02 ± 3.98	.969
	*D*slow	1.20 ± 0.23	1.54 ± 0.31	.000***	1.18 ± 0.22	1.56 ± 0.30	.000***
	*D*fast	8.01 ± 1.71	8.10 ± 2.89	.781	8.24 ± 2.06	7.48 ± 1.96	.253
	$T2_{Dvery\text{-}slow}$	213.77 ± 79.25	320.06 ± 165.32	.008**	211.45 ± 74.53	320.81 ± 165.54	.004**
	$T2_{Dslow}$	107.39 ± 21.74	132.45 ± 22.95	.000***	107.27 ± 19.94	131.47 ± 27.43	.001**
	$T2_{Dfast}$	946.51 ± 177.29	1018.41 ± 216.08	.178	932.66 ± 181.13	1052.54 ± 186.25	.019*

The parameters ADC, D_{slow}, and D_{fast} are measured in units of $\times 10^{-3}$ mm^2/s, $F_{Dvery\text{-}slow}$, F_{Dslow} and F_{Dfast} are measured in percentages (%), while $T2_{global}$, $T2_{Dvery\text{-}slow}$, $T2_{Dslow}$, $T2_{Dfast}$ are measured in milliseconds (ms)

Mono-exp mono-exponential, *HM-MRI* hybrid multidimensional, *HGGs* high grade gliomas, *LGGs* low grade gliomas, *IDH* isocitrate dehydrogenase, *IDH-WILD* IDH wild type gliomas, *IDH-MUT* IDH mutant type gliomas, *ADC* apparent diffusion coefficient, T2global global mean T2 value

*$p < .05$

**$p < .01$

***$p < .001$

Table 5 ROC analysis of each MRI-derived metric and their combinations in grading and predicting IDH mutation status of gliomas

Model	Metrics	AUC value	Cut-off value	95% CI	Sensitivity (%)	Specificity (%)
Grading gliomas						
Mono-exp	*ADC*	0.808	0.468	0.688–0.928	77.8	77.4
	$T2_{global}$	0.784	123.311	0.664–0.904	77.8	79.2
	$ADC + T2_{global}$	0.808	0.220	0.688–0.928	77.8	77.4
HM-MRI	$F_{Dvery\text{-}slow}$	0.854	7.4	0.740–0.969	86.8	83.3
	F_{Dslow}	0.705	79.8	0.564–0.847	72.2	64.2
	*D*slow	0.816	1.446	0.686–0.945	66.7	90.6
	$T2_{Dvery\text{-}slow}$	0.711	294.458	0.562–0.859	55.6	88.7
	$T2_{Dslow}$	0.790	120.441	0.671–0.910	77.8	81.1
	$T2_{Dfast}$	0.607	961.394	0.451–0.763	66.7	58.5
	Combination	0.876	0.323	0.774–0.979	77.8	92.5
Predicting IDH mutation status						
Mono-exp	*ADC*	0.819	0.507	0.691–0.947	73.7	86.5
	$T2_{global}$	0.778	127.524	0.647–0.910	73.7	84.6
	$ADC + T2_{global}$	0.819	0.304	0.691–0.947	73.7	86.5
HM-MRI	$F_{Dvery\text{-}slow}$	0.821	8.0	0.692–0.950	78.9	80.8
	F_{Dslow}	0.691	79.8	0.560–0.823	68.4	63.5
	*D*slow	0.845	1.396	0.727–0.963	73.7	90.4
	$T2_{Dvery\text{-}slow}$	0.723	294.458	0.587–0.859	52.6	88.5
	$T2_{Dslow}$	0.763	120.441	0.615–0.911	78.9	82.7
	$T2_{Dfast}$	0.682	961.394	0.538–0.827	73.7	61.5
	Combination	0.845	0.318	0.727–0.963	73.7	90.4

Mono-exp mono-exponential, *HM-MRI* hybrid multi-dimensional MRI, *Combination* a combination of HM-MRI metrics, *ADC* apparent diffusion coefficient, $T2_{global}$ global mean T2 value

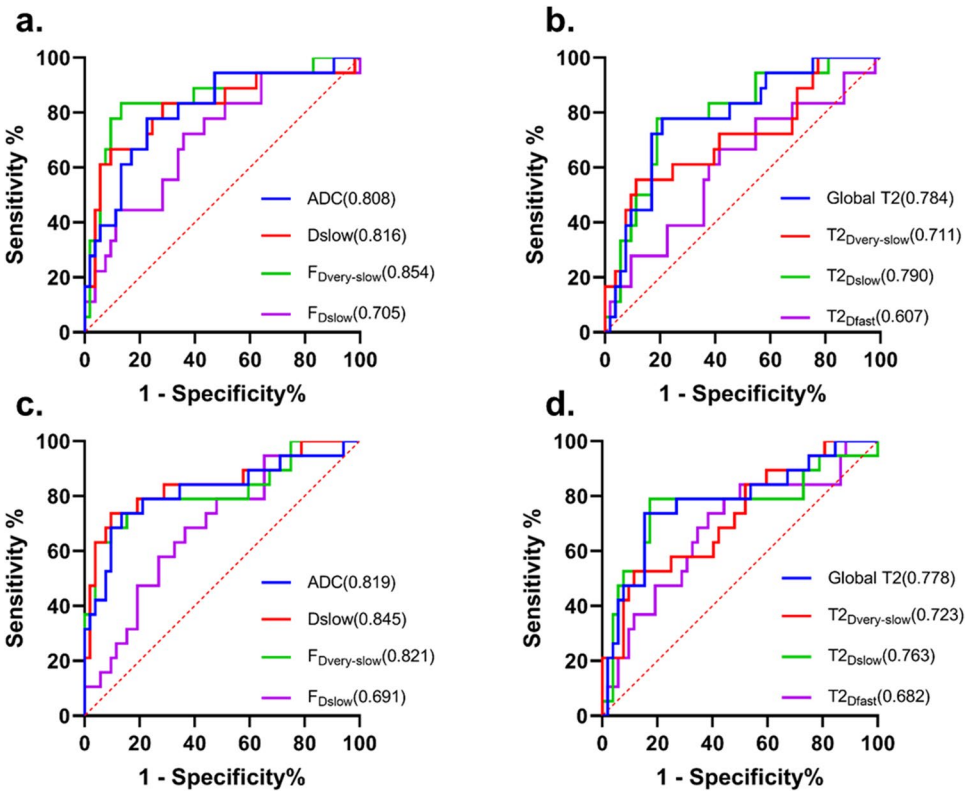

Fig. 5 Graph shows the ROC curves of each parameter for grading gliomas (**a**, **b**) and discrimination between the IDH-wild group and the IDH-mutant group (**c**, **d**). The highest AUC in grading was observed with the $F_{D\text{very-slow}}$, while the highest AUC in predicting IDH mutation status was observed with the *D*slow. AUC, area under curve

component could capture fluid in both EES and vessels and corresponded to the background area in the H&E staining. And $F_{D\text{fast}}$'s low specificity may restrict its diagnostic performance. By correlating HM-MRI metrics with quantitative H&E results, our study provided a pathological perspective of the fraction metrics, which has not been reported in previous three-compartment diffusion studies [24, 27].

Mono-exponential model metrics, such as ADC and T2 map, have been extensively studied for their potential in clinic. Several studies have already used ADC or T2 map alone for grading and predicting IDH mutation status, and showed modest to good performance for ADC [9–11] and T2 [12, 13]. However, both ADC and T2 are complex reflections of the heterogeneity of tumor tissues within a voxel, which may limit their diagnostic performance. Compared with ADC alone, T2 alone or their combination, this study manifested that HM-MRI metric $F_{D\text{very-slow}}$ achieved a higher AUC in grading gliomas. This might be due to that $F_{D\text{very-slow}}$ is a sub-voxel metric, which is correlated with the histologic features within a voxel. This study also found that the HM-MRI metric *D*slow had a greater AUC than the ADC in diagnosing IDH mutation status. *D*slow's superior performance could be attributed to the fact that it reflected the diffusion coefficient of stromal areas, and the extracellular matrix of the tumor microenvironment in IDH-mutant and IDH-wild gliomas could differ significantly. Furthermore, in this study, the LR analysis revealed that the combination of HM-MRI metrics $F_{D\text{very-slow}}$ and $T2_{D\text{slow}}$ further improved the performance in grading gliomas. This improvement might be due to that the HM-MRI provides not only diffusion information, but also fraction and T2 information at the sub-voxel level.

More specifically, by combining HM-MRI with the modified three-compartment model, this study showed that HM-MRI was able to resolve microenvironments that possess comparable ADC but different T2 values or similar T2 values but different ADC. Therefore, it was able to solve the drawbacks of DWI in detecting tumor lesions with T2-shine-through and T2-blackout effects, as shown in Fig. 2. Besides, our HM-MRI approach revealed that $T2_{D\text{very-slow}}$, $T2_{D\text{slow}}$ and $T2_{D\text{fast}}$ were all significantly lower in IDH-wild gliomas than in IDH-mutant gliomas. Our observations in $T2_{D\text{very-slow}}$, $T2_{D\text{slow}}$ and $T2_{D\text{fast}}$ could be attributed to differences in the compositions of the microenvironment within the intracellular space, EES, and intravascular space between IDH-wild and IDH-mutant gliomas. It is possible that more severe disruption of the BBB in IDH-wild gliomas compared to IDH-mutant gliomas allows for more leakage of plasma substances into the EES [28]. Additionally, cytokines, chemokines, and metabolites secreted within tumor microenvironment could be different between IDH-wild and IDH-mutant gliomas, which may also contribute to the observed differences in T2 values. For instance, IDH mutation might lead to the production of the 2-hydroxyglutarate (2-HG) and increased levels of

nicotinamide adenine dinucleotide phosphate (NADPH) [29]. As a result, our findings indicate the potential value of HM-MRI in the clinic by reflecting some information relating to the compositions across different compartments within the tumor microenvironment via T2 values, in addition to the microstructure features of gliomas tissues via fractions and diffusion coefficients.

Several limitations of this study should be acknowledged. First, HM-MRI in this study had a small coverage (only 7 slices) and long scanning time (8min20sec). This acquisition limitation could be addressed using more efficient strategies, such as simultaneous multi-slice (SMS) [30] and ZEBRA acceleration [31]. Second, the ROI-based method used in this study was operator-dependent and may have introduced some bias. Third, despite a simple semi-quantitative method was employed for histologic evaluations, we still faced challenges in distinguishing boundaries between glioma cells and stroma cells through H&E staining. In the future, quantitative methods may be needed to analyze H&E staining or IHC results and to find more correlations between histologic findings with the HM-MRI metrics. Besides, it should be highlighted that all HM-MRI metrics were based on a whole tumor analysis, while histology evaluations were performed on a certain sample. Although we did found some correlation, further biopsy studies under MRI-guided navigation and a voxel-matched comparison is necessary. Finally, while we conducted this work at 3.0 T, it is worth noting that this HM-MRI approach is equally applicable at 1.5 T. Because biological tissues at 1.5 T have a longer T2 and fewer susceptibility artifacts than at 3.0 T, this HM-MRI approach may have some advantage at 1.5 T over 3.0 T, particularly for detecting bleeding lesions with short T2. Further research at 1.5 T is required to corroborate our idea.

In conclusion, our study highlights the promise of HM-MRI as a valuable non-invasive diagnostic tool in the management of gliomas, by correlating HM-MRI metrics with quantitative H&E staining results, grading and predicting the IDH mutation status.

Acknowledgements This work was partly supported by the National NSFC International (regional) Cooperation and Exchange Project (Grant No. 82111530204), partly supported by Swedish Foundation for International Cooperation in Research and Higher Education (Grant No. CH2020-8775), and partly supported by Hubei Provincial Natural Science Foundation of China (Grant No. 2021CFB099).

Author contributions Wenbo Sun: investigation; data curation; validation; writing—original draft; visualization; formal analysis**.** Dan Xu: investigation; data curation; validation; writing—original draft; visualization; formal analysis. Huan Li: data curation; project administration**.** Sirui Li: investigation; methodology. QingJia Bao: writing—review & editing; resources. Xiaopeng Song: software; resources. Daniel Topgaard: supervision; conceptualization; funding acquisition; writing-review & editing. Haibo Xu: supervision; conceptualization; funding acquisition; writing—review & editing.

Data availability For ethical considerations, the data supporting the study's conclusions are not publicly available; however, they are available from the corresponding author upon appropriate request.

Declarations

Conflict of interest The authors declare no conflict of interest.

Ethical statement All enrolled subjects provided informed consent, and the ethics committee of our hospital approved this prospective study (Ethics number 2020109).

References

1. Burgenske DM, Yang J, Decker PA et al (2019) Molecular profiling of long-term IDH-wildtype glioblastoma survivors. Neuro Oncol. https://doi.org/10.1093/neuonc/noz129
2. Gritsch S, Batchelor TT, Gonzalez Castro LN (2022) Diagnostic, therapeutic, and prognostic implications of the 2021 World Health Organization classification of tumors of the central nervous system. Cancer. https://doi.org/10.1002/cncr.33918
3. Komori T (2022) Grading of adult diffuse gliomas according to the 2021 WHO classification of tumors of the central nervous system. Lab Invest. https://doi.org/10.1038/s41374-021-00667-6
4. Louis DN, Perry A, Wesseling P et al (2021) The 2021 WHO classification of tumors of the central nervous system: a summary. Neuro Oncol. https://doi.org/10.1093/neuonc/noab106
5. Uribe-Cardenas R, Giantini-Larsen AM, Garton A, Juthani RG, Schwartz TH (2022) Innovations in the diagnosis and surgical management of low-grade gliomas. World Neurosurg. https://doi.org/10.1016/j.wneu.2022.06.070
6. Szychot E, Youssef A, Ganeshan B et al (2021) Predicting outcome in childhood diffuse midline gliomas using magnetic resonance imaging based texture analysis. J Neuroradiol. https://doi.org/10.1016/j.neurad.2020.02.005
7. Narvaez O, Svenningsson L, Yon M, Sierra A, Topgaard D (2022) Massively multi-dimensional diffusion-relaxation correlation MRI. Front Phys. https://doi.org/10.3389/fphy.2021.793966
8. Jalnefjord O, Andersson M, Montelius M et al (2018) Comparison of methods for estimation of the intravoxel incoherent motion (IVIM) diffusion coefficient (D) and perfusion fraction (f). MAGMA. https://doi.org/10.1007/s10334-018-0697-5
9. Hu LS, Hawkins-Daarud A, Wang L, Li J, Swanson KR (2020) Imaging of intratumoral heterogeneity in high-grade glioma. Cancer Lett. https://doi.org/10.1016/j.canlet.2020.02.025
10. Guo D, Jiang B (2023) Noninvasively evaluating the grade and IDH mutation status of gliomas by using mono-exponential, bi-exponential diffusion-weighted imaging and three-dimensional pseudo-continuous arterial spin labeling. Eur J Radiol. https://doi.org/10.1016/j.ejrad.2023.110721
11. Maynard J, Okuchi S, Wastling S et al (2020) World Health Organization grade II/III glioma molecular status: prediction by MRI morphologic features and apparent diffusion coefficient. Radiology. https://doi.org/10.1148/radiol.2020191832
12. Gu W, Fang S, Hou X, Ma D, Li S (2021) Exploring diagnostic performance of T2 mapping in diffuse glioma grading. Quant Imaging Med Surg. https://doi.org/10.21037/qims-20-916
13. Kern M, Auer TA, Picht T, Misch M, Wiener E (2020) T2 mapping of molecular subtypes of WHO grade II/III gliomas. BMC Neurol. https://doi.org/10.1186/s12883-019-1590-1
14. Cao M, Ding W, Han X et al (2019) Brain T1ρ mapping for grading and IDH1 gene mutation detection of gliomas: a preliminary study. J Neurooncol. https://doi.org/10.1007/s11060-018-03033-7

15. Springer E, Cardoso PL, Strasser B et al (2022) MR fingerprinting—a radiogenomic marker for diffuse gliomas. Cancers (Basel). https://doi.org/10.3390/cancers14030723
16. Auer TA, Kern M, Fehrenbach U et al (2021) T2 mapping of the peritumoral infiltration zone of glioblastoma and anaplastic astrocytoma. Neuroradiol J. https://doi.org/10.1177/19714009219893325
17. Bontempi P, Rozzanigo U, Amelio D et al (2021) Quantitative multicomponent T2 relaxation showed greater sensitivity than flair imaging to detect subtle alterations at the periphery of lower grade gliomas. Front Oncol. https://doi.org/10.3389/fonc.2021.651137
18. Toh CH, Chen YL, Hsieh TC et al (2006) Glioblastoma multiforme with diffusion-weighted magnetic resonance imaging characteristics mimicking primary brain lymphoma. case report. J Neurosurg. https://doi.org/10.3171/jns.2006.105.1.132
19. Kim Y, Lee SK, Kim JY, Kim JH (2023) Pitfalls of diffusion-weighted imaging: clinical utility of T2 shine-through and T2 black-out for musculoskeletal diseases. Diagnostics (Basel). https://doi.org/10.3390/diagnostics13091647
20. Chatterjee A, Mercado C, Bourne RM et al (2022) Validation of prostate tissue composition by using hybrid multi-dimensional MRI: correlation with histologic findings. Radiology. https://doi.org/10.1148/radiol.2021204459
21. Chatterjee A, Antic T, Gallan AJ et al (2022) Histological validation of prostate tissue composition measurement using hybrid multi-dimensional MRI: agreement with pathologists' measures. Abdom Radiol (NY). https://doi.org/10.1007/s00261-021-03371-7
22. Lee GH, Chatterjee A, Karademir I et al (2022) Comparing radiologist performance in diagnosing clinically significant prostate cancer with multiparametric versus hybrid multi-dimensional MRI. Radiology. https://doi.org/10.1148/radiol.211895
23. Zeng Q, Shi F, Zhang J, Ling C, Dong F, Jiang B (2018) A modified tri-exponential model for multi-b-value diffusion-weighted imaging: a method to detect the strictly diffusion-limited compartment in brain. Front Neurosci. https://doi.org/10.3389/fnins.2018.00102
24. Cao M, Wang X, Liu F, Xue K, Dai Y, Zhou Y (2023) A three-component multi-b-value diffusion-weighted imaging might be a useful biomarker for detecting microstructural features in gliomas with differences in malignancy and IDH-1 mutation status. Eur Radiol. https://doi.org/10.1007/s00330-022-09212-5
25. Yushkevich PA, Piven J, Hazlett HC et al (2006) User-guided 3D active contour segmentation of anatomical structures: significantly improved efficiency and reliability. Neuroimage. https://doi.org/10.1016/j.neuroimage.2006.01.015
26. Boruah D, Deb P, Srinivas V, Mani NS (2014) Morphometric study of nuclei and microvessels in gliomas and its correlation with grades. Microvasc Res. https://doi.org/10.1016/j.mvr.2014.03.002
27. Zaccagna F, Riemer F, Priest AN et al (2019) Non-invasive assessment of glioma microstructure using VERDICT MRI: correlation with histology. Eur Radiol. https://doi.org/10.1007/s00330-019-6011-8
28. Raja R, Rosenberg GA, Caprihan A (2018) MRI measurements of blood-brain barrier function in dementia: a review of recent studies. Neuropharmacology. https://doi.org/10.1016/j.neuropharm.2017.10.034
29. Yan H, Parsons DW, Jin G et al (2009) IDH1 and IDH2 mutations in gliomas. N Engl J Med. https://doi.org/10.1056/NEJMoa0808710
30. Furtado FS, Mercaldo ND, Vahle T et al (2023) Simultaneous multislice diffusion-weighted imaging versus standard diffusion-weighted imaging in whole-body PET/MRI. Eur Radiol. https://doi.org/10.1007/s00330-022-09275-4
31. Slator PJ, Palombo M, Miller KL et al (2021) Combined diffusion-relaxometry microstructure imaging: current status and future prospects. Magn Reson Med. https://doi.org/10.1002/mrm.28963